PROCEEDINGS OF SCIENCE

First measurements from charmless B decays at Belle II

Yun-Tsung Lai[*†]
Kavli IPMU
E-mail: yun-tsung.lai@ipmu.jp

We report on first measurements of branching fractions, *CP*-violating charge-asymmetries, and polarizations in various charmless B decays at Belle II. We use a sample of electron-positron collisions collected in 2019–2020 at the $\Upsilon(4S)$ resonance from the SuperKEKB collider corresponding to an integrated luminosity of 34.6 fb^{-1}. All results are consistent with known values and provide extensive validations of the detector performances and analysis strategies.

The 19th International Conference on B-Physics at Frontier Machines (BEAUTY 2020)
21-24 September, 2020
Remote conference

[*] Speaker.
[†] On behalf of the Belle II Collaboration.

1. Introduction

Charmless B decays are important to search for non-standard-model (non-SM) physics in the flavor sector. Many decay channels are governed by 'penguin' amplitudes, which are sensitive to non-SM contributions to the loop. Studying them in detail is an important goal of the Belle II experiment. With the largest sample of e^+e^- collisions expected in the next decade, Belle II is expected to improve significantly important measurements such as the determination of the CKM phase α/ϕ_2 [1, 2], the precision test of of $K\pi$ isospin sum rule [1, 3], and the study of CP-violating asymmetries localized in the three-body B decays' phase space [1]. In addition, the measurement of decay-time dependent CP violation in the penguin-dominated $B^0 \to \phi K^0$ mode, compared with corresponding results from $B^0 \to J/\psi K^0$ decays, will offer a sharp probe of non-SM physics. Measurements of the longitudinal polarization fractions (f_L) of decays of B mesons into pairs of vector mesons also probe non-SM dynamics. Previous measurements of f_L in $B^0 \to J/\psi K^0$ showed a sizable contribution from transverse polarization, while most predictions expect the longitudinal component to dominate. Further, more precise f_L measurements may shed light on the issue.

SuperKEKB [6] is an asymmetric e^+e^+ collider, which started collision operations with the Belle II detector [7] in March 2019. We use a data sample of 34.6 fb^{-1}, which was collected at the Υ(4S) resonance up to May 2020. This report presents the first measurements of branching fractions ($\mathscr{B}$), CP-violating charge-asymmetries ($\mathscr{A}_{CP}$), and longitudinal polarization fractions (f_L) based on the following B decays reconstructed in Belle II data: $B^0 \to K^+\pi^-$, $B^0 \to \pi^+\pi^-$, $B^+ \to K^+\pi^0$, $B^+ \to \pi^+\pi^0$, $B^+ \to K^0\pi^+$, $B^0 \to K^0\pi^0$, $B^+ \to K^+K^-K^+$, $B^+ \to K^+\pi^-\pi^+$, $B^0 \to \phi K^0$, $B^+ \to \phi K^+$, $B^0 \to \phi K^{*0}$, and $B^{*+} \to \phi K^{*+}$ [8, 9].

The B reconstruction, event seletion criteria, and background suppression strategy are studied with various simulated signal and background samples. Charged-particle trajectories (tracks) are identified with inner vertex detectors and a central drift chamber with requirements on the displacement from the interaction point to reduce beam-background-induced tracks. The identification of charged particles uses the information from two particle-identification (PID) devices, a time-of-propagation counter in the barrel region and a proximity-focusing aerogel ring-image Cherenkov counter in the forward endcap region. Decays of π^0 candidates are reconstructed by using two isolated clusters in the electromagnetic calorimeter, with requirements on the helicity angle and kinematic-fit quality to constrain π^0 mass. Decays of K_S^0 candidates are reconstructed from two opposite-charge pion candidates from a common vertex, restricted to meet additional requirements on their kinematic variables, e.g., momentum, flight distance, distance between pion trajectories, to further reduce the combinatorial background. Decays of ϕ candidates are reconstructed from two opposite-charge kaon candidates. Decays of K^{*0} candidates are reconstructed from one K^+ and one π^-, and decays of K^{*+} candidates are reconstructed from one K_S^0 and one π^+. In three-body decays, we suppress the relevant peaking backgrounds from charmed or charmonium intermediate states by excluding the corresponding two-body mass ranges.

We use the following two variables to distinguish the signal B events from other backgrounds: the energy difference $\Delta E \equiv E_B - \sqrt{s}/2$ between the reconstructed B candidate and half of the collision energy in the $\Upsilon(4S)$ frame, and beam-energy-constrained mass $M_{\rm bc} \equiv \sqrt{s/(4c^2) - (p_B^*/c)^2}$.

2. Continuum background suppression

One of the main challenges of charmless B decays' reconstruction is the large combinatorial background with the same final state from $e^+e^- \to q\overline{q}$ ($q = u,d,s,c$) processes. Signal rates 10^5 times smaller than continuum background and the lack of distinctive final-state features (leptons or intermediate resonances) make the reconstruction of signal hard. A binary boosted decision-tree (BDT) classifier is used to combine more than 30 variables nonlinearly. The input variables to the BDT include event topology variables, flavor-tagging information, vertex-fitting information, and kinematic-fit information. All of them are required to be loosely or not correlated to ΔE and $M_{\rm bc}$.

3. Signal extraction and measurement results

We use unbinned maximum likelihood fits to extract signal yields from the data to calculate various physics observables. In the $B \to hh$ and $B \to hhh$ ($h = K$ or π) analyses, only ΔE is fit for events restricted to $M_{\rm bc} > 5.27$ GeV/c^2. The fits to the two $B \to \phi K$ modes use five variables including ΔE, $M_{\rm bc}$, output of the continuum suppression BDT discriminator (C'_{out}), K^+K^- candidate mass ($m_{K^+K^-}$), and ϕ candidate's cosine of the helicity angle ($\cos\theta_{H,\phi}$). The fits to the two $B \to \phi K^*$ modes use seven variables: $K^+\pi^-$ candidate mass ($m_{K\pi}$) and K^* candidate's cosine of the helicity angle ($\cos\theta_{H,K^*}$) in addition to the ones used in $B \to \phi K$ modes. By fitting data, we determine the following quantities:

- Branching fractions: $\mathscr{B} = \frac{N}{\varepsilon \times 2 \times N_{BB}}$, where N is the signal yield, ε is the signal reconstruction efficiency determined from simulation and validated with control samples, and N_{BB} is the number of $B\overline{B}$ events (19.7×10^6 for B^+B^- and 18.7×10^6 for $B^0\overline{B}^0$). N_{BB} is obtained from the measured integrated luminosity, the exclusive $e^+e^- \to \Upsilon(4S)$ cross section, and $\mathscr{B}(\Upsilon(4S) \to B^0\overline{B}^0)$ [10].

- CP asymmetries: The raw asymmetries are obtained as $\mathscr{A} = \frac{N(b)-N(\overline{b})}{N(b)+N(\overline{b})}$, where $N(b)$ and $N(\overline{b})$ are the yields of the final-state mesons containing b and $\overline{b}$ flavors, respectively. The CP asymmetry is obtained by correcting the observed asymmetry $\mathscr{A}$ for the instrumental asymmetry $\mathscr{A}_{CP} = \mathscr{A} - \mathscr{A}_{det}$, where $\mathscr{A}_{det}(K^+\pi^-) = -0.010 \pm 0.003$ and $\mathscr{A}_{det}(K^0_S\pi^+) = -0.007 \pm 0.022$ are measured on large samples of $D^0 \to K^-\pi^+$ and $D^+ \to K^0_S\pi^+$ decays with negligible CP violation. Then $\mathscr{A}_{det}(K^+)$ is determined as $\mathscr{A}_{det}(K^+) = \mathscr{A}_{det}(K^+\pi^-) - \mathscr{A}_{det}(K^0_S\pi^+) + \mathscr{A}_{det}(K^0_S) = -0.015 \pm 0.022$ where an upper bound on $\mathscr{A}_{det}(K^0_S)$ is used based on previous measurements [11].

- Longitudinal polarization fractions: $f_L = \frac{N_L/\varepsilon_L}{N_L/\varepsilon_L + N_T/\varepsilon_T}$, where $N_{L(T)}$ and $\varepsilon_{L(T)}$ are the signal yield and signal reconstruction efficiency with longitudinal (transverse) polarization, respectively. The distinctive helicity-angle distributions allow for separating the two signal components.

Figures 1–8 show the ΔE distributions in data for $B^0 \to K^+\pi^-$, $B^0 \to \pi^+\pi^-$, $B^+ \to K^+\pi^0$, $B^+ \to \pi^+\pi^0$, $B^+ \to K^0\pi^+$, $B^0 \to K^0\pi^0$, $B^+ \to K^+K^-K^+$, and $B^+ \to K^+\pi^-\pi^+$ decays, with fit projections overlaid. Figure 9 shows the ΔE, $M_{\rm bc}$, C'_{out}, $m_{K^+K^-}$, and $\cos\theta_{H,\phi}$ distributions in data for $B^+ \to \phi K^+$ and $B^0 \to \phi K^0$ decays, with fit projections overlaid. Figure 10 shows the ΔE, $M_{\rm bc}$,

C'_{out}, $m_{K^+K^-}$, $\cos\theta_{H,\phi}$, $m_{K\pi}$, and $\cos\theta_{H,K^*}$ distributions in data for $B^+ \to \phi K^{*+}$ and $B^0 \to \phi K^{*0}$ decays, with fit projections overlaid. The major systematic uncertainties come from tracking, PID, and fit modelling. All the measurement results are summarized in Table 1.

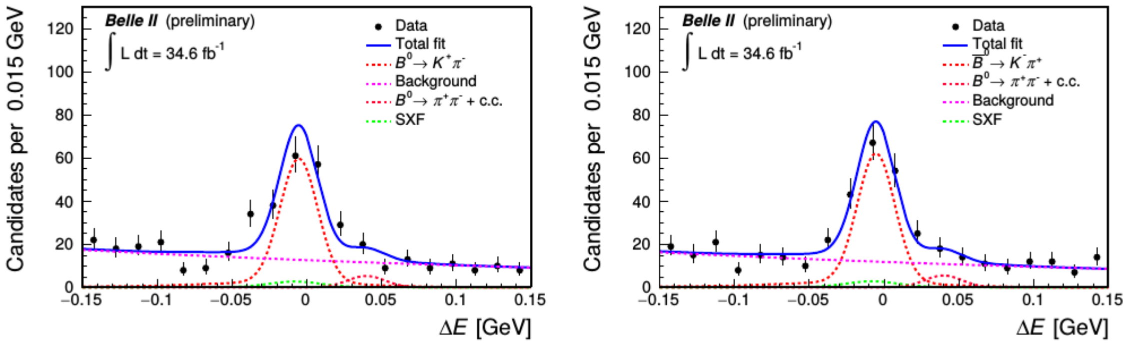

Figure 1: Distribution of ΔE for $B^0 \to K^+\pi^-$ (left) and $\overline{B}^0 \to K^-\pi^+$ (right) decays with fit projections overlaid.

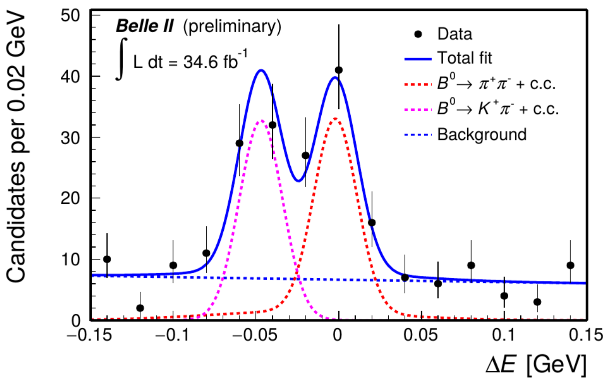

Figure 2: Distribution of ΔE for $B^0 \to \pi^+\pi^-$ decays with fit projections overlaid.

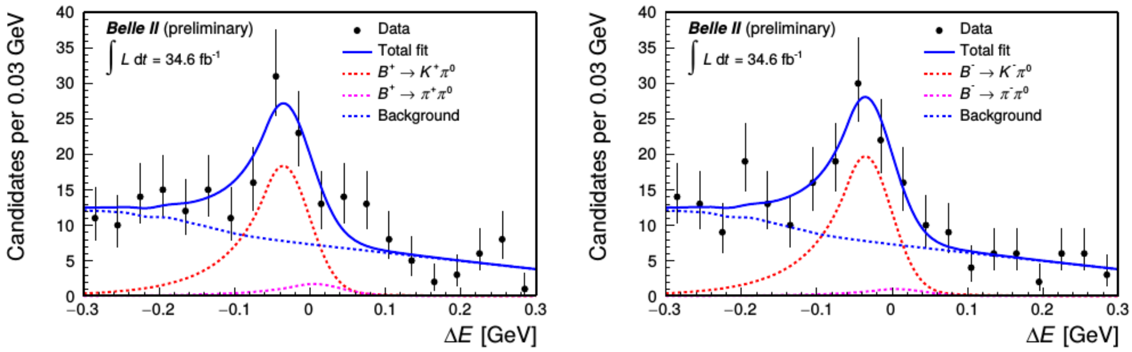

Figure 3: Distribution of ΔE for $B^+ \to K^+\pi^0$ (left) and $B^- \to K^-\pi^0$ (right) decays with fit projections overlaid.

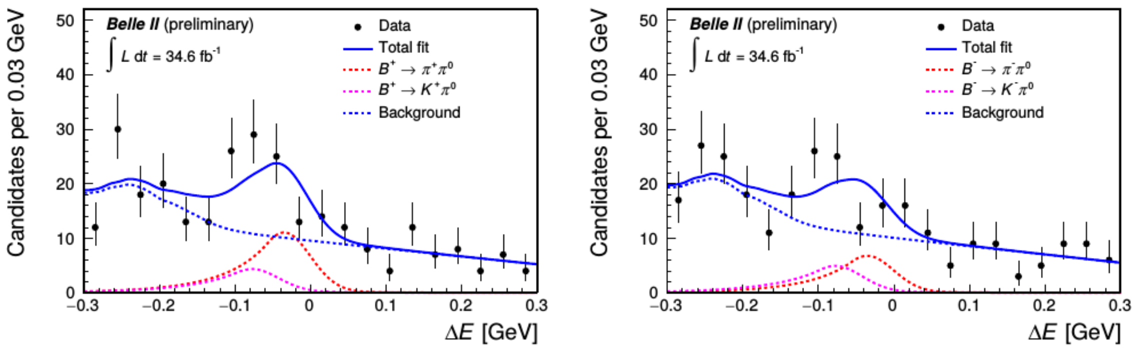

Figure 4: Distribution of ΔE for $B^+ \to \pi^+\pi^0$ (left) and $B^- \to \pi^-\pi^0$ (right) decays with fit projections overlaid.

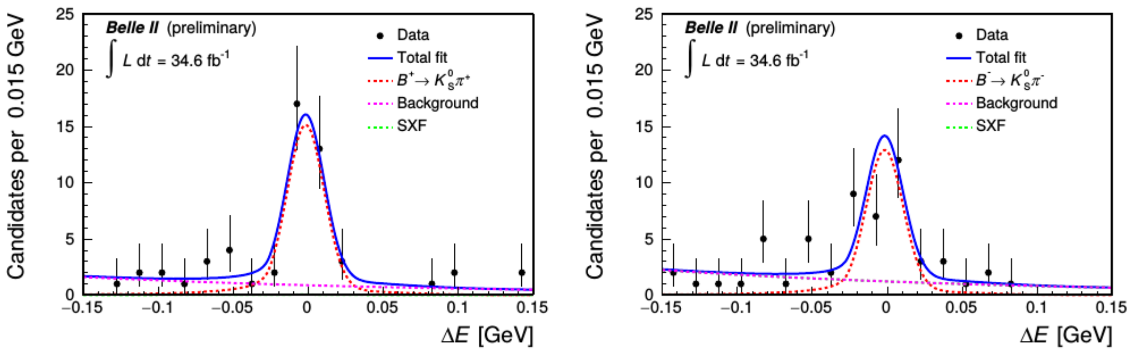

Figure 5: Distribution of ΔE for $B^+ \to K^0_S\pi^+$ (left) and $B^- \to K^0_S\pi^-$ (right) decays with fit projections overlaid.

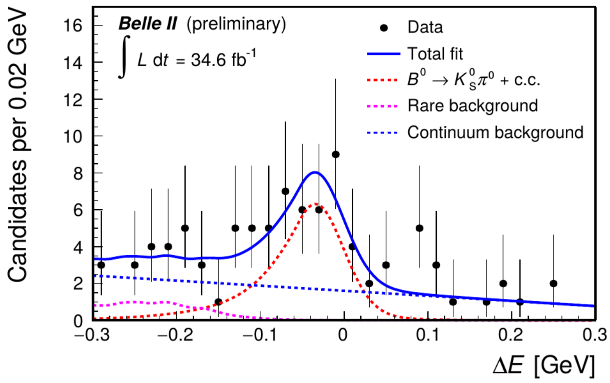

Figure 6: Distribution of ΔE for $B^0 \to K_S^0\pi^0$ decays with fit projections overlaid.

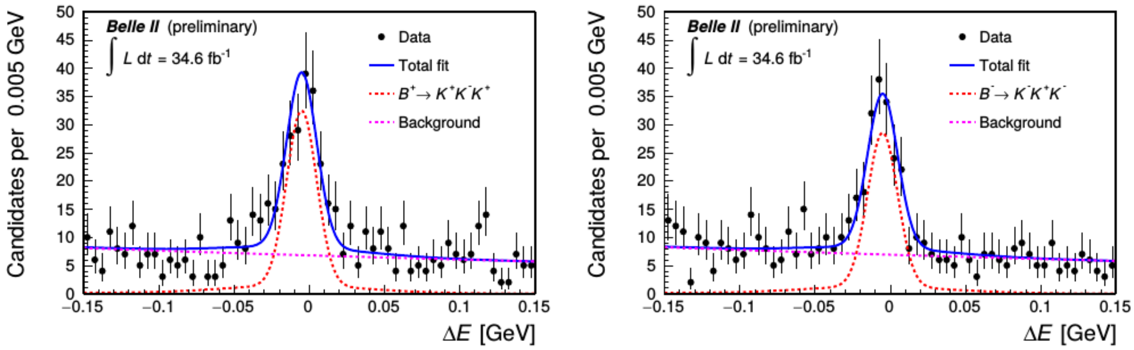

Figure 7: Distribution of ΔE for $B^+ \to K^+K^-K^+$ (left) and $B^- \to K^-K^+K^-$ (right) decays with fit projections overlaid.

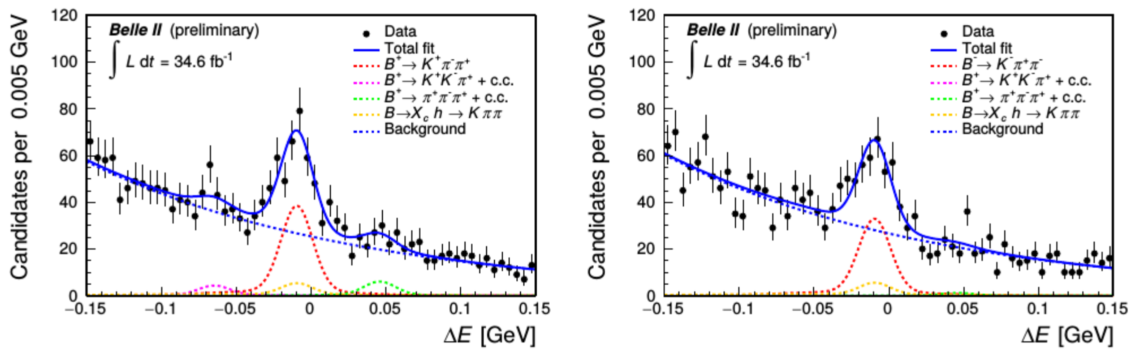

Figure 8: Distribution of ΔE for $B^+ \to K^+\pi^-\pi^+$ (left) and $B^- \to K^-\pi^+\pi^-$ (right) decays with fit projections overlaid.

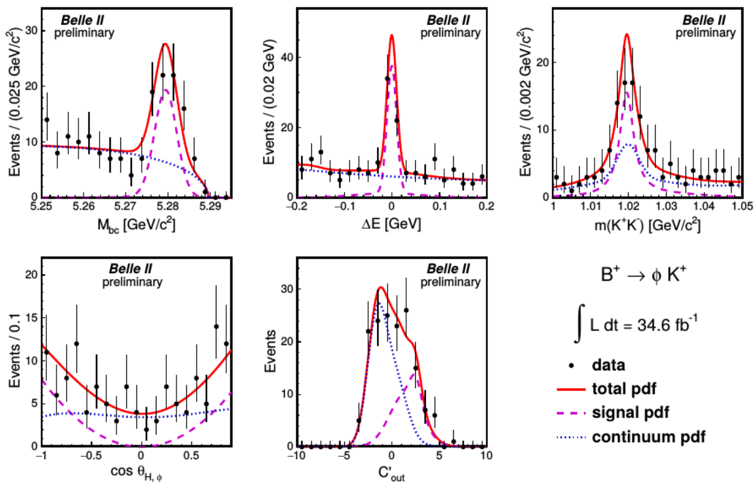

(a) $B^+ \to \phi K^+$

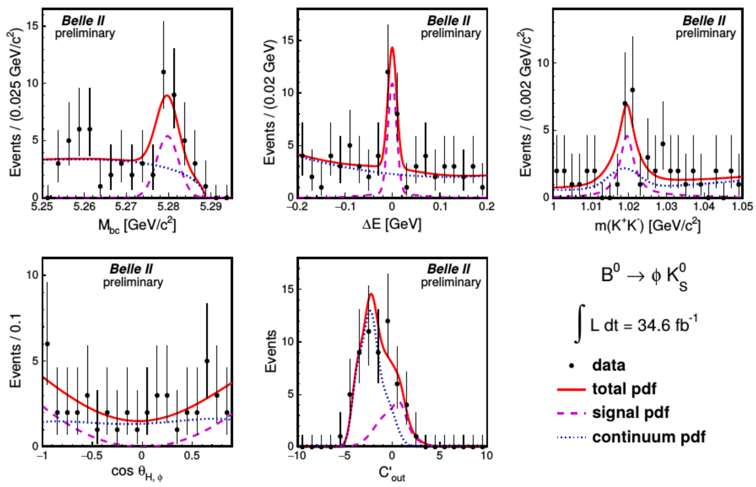

(b) $B^0 \to \phi K^0$

Figure 9: Distribution of ΔE, $M_{\rm bc}$, C'_{out}, $m_{K^+K^-}$, and $\cos\theta_{H,\phi}$ for $B^+ \to \phi K^+$ and $B^0 \to \phi K^0$ decays with fit projections overlaid.

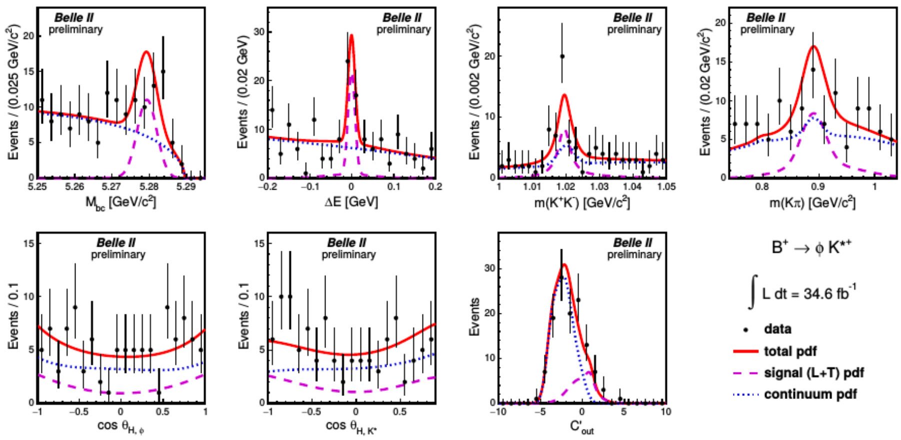

(a) $B^+ \to \phi K^{*+}$

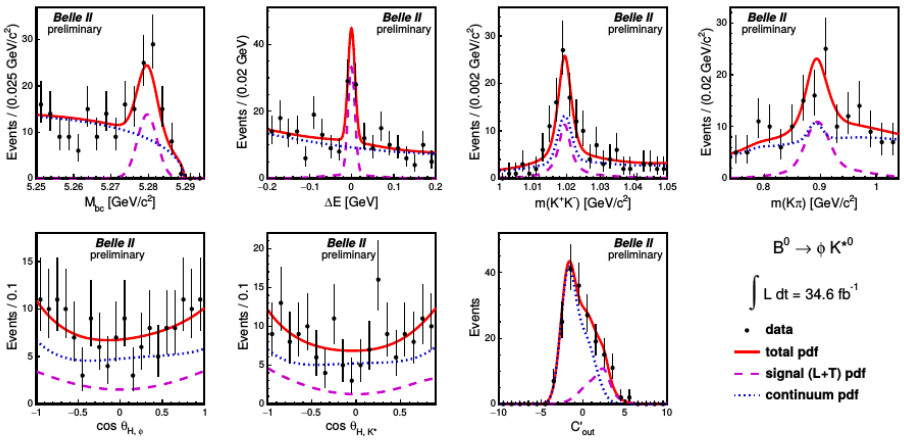

(b) $B^0 \to \phi K^{*0}$

Figure 10: Distribution of ΔE, $M_{\rm bc}$, C'_{out}, $m_{K^+K^-}$, $\cos\theta_{H,\phi}$, $m_{K\pi}$, and $\cos\theta_{H,K^*}$ for $B^+ \to \phi K^{*+}$ and $B^0 \to \phi K^{*0}$ decays with fit projections overlaid.

Table 1: Summary of measurement results. The first uncertainties are statistical and the second ones are systematic.

Mode	$\mathscr{B}$ (10^{-6})	$\mathscr{A}_{CP}$	f_L
$B^0 \to K^+\pi^-$	$18.9 \pm 1.4 \pm 1.0$	$0.030 \pm 0.064 \pm 0.008$	-
$B^0 \to \pi^+\pi^-$	$5.6^{+1.0}_{-0.9} \pm 0.3$	-	-
$B^+ \to K^+\pi^0$	$12.7^{+2.2}_{-2.1} \pm 1.1$	$0.052^{+0.121}_{-0.119} \pm 0.022$	-
$B^+ \to \pi^+\pi^0$	$5.7 \pm 2.3 \pm 0.5$	$-0.268^{+0.249}_{-0.322} \pm 0.123$	-
$B^+ \to K^0\pi^+$	$21.8^{+3.3}_{-3.0} \pm 2.9$	$-0.072^{+0.109}_{-0.114} \pm 0.024$	-
$B^0 \to K^0\pi^0$	$10.9^{+2.9}_{-2.6} \pm 1.6$	-	-
$B^+ \to K^+K^-K^+$	$32.0 \pm 2.2 \pm 1.4$	$-0.049 \pm 0.063 \pm 0.022$	-
$B^+ \to K^+\pi^-\pi^+$	$48.0 \pm 3.8 \pm 3.3$	$-0.063 \pm 0.081 \pm 0.023$	-
$B^0 \to \phi K^0$	$5.9 \pm 1.8 \pm 0.7$	-	-
$B^+ \to \phi K^+$	$6.7 \pm 1.1 \pm 0.5$	-	-
$B^0 \to \phi K^{*0}$	$11.0 \pm 2.1 \pm 1.1$	-	$0.57 \pm 0.20 \pm 0.04$
$B^{*+} \to \phi K^{*+}$	$21.7 \pm 4.6 \pm 1.9$	-	$0.58 \pm 0.23 \pm 0.02$

4. Summary

Belle II reports first measurements in charmless B decays with a data sample corresponding to 34.6 fb^{-1}. The measurements include branching fractions, CP asymmetries, and longitudinal polarization fractions. All the results are in agreement with the known values, and offer good validation on the detector performance and analysis strategies.

References

[1] E. Kou *et al.* (Belle II Collaboration), PTEP **2019** (2019) no.12, 123C01, arXiv:1808.10567 [hep-ex].

[2] M. Gronau and D. London, Phys. Rev. Lett. **65** (1990) 3381 .

[3] M. Gronau, Phys. Lett. B **627** (2005) no. 1, 82-88.

[4] A. L. Kagan, Phys. Lett. B **601** (2004) no. 3 151-163.

[5] M. Beneke, J. Rohrer, and D. Yang, Phys. Rev. Lett. **96** (2006) 141801.

[6] K. Akai *et al.*, Nucl. Instrum. Meth. A **907** (2018) 188-199 .

[7] T. Abe *et al.* (Belle II Collaboration), arXiv:1011.0352 [hep-ex].

[8] F. Abudinén (Belle II Collaboration), arXiv:2009.09452 [hep-ex].

[9] F. Abudinén (Belle II Collaboration), arXiv:2008.03873 [hep-ex].

[10] A. J. Bevan *et al.* (Belle and BaBar Collaborations), Eur. Phys. J. **C74** (2014) 3026, arXiv:1406.6311 [hep-ex].

[11] A. Davis *et al.* (LHCb Collaboration), [LHCb-PUB-2018-004].